ELSEVIER

Journal of Chromatography A, 945 (2002) 65–81

JOURNAL OF CHROMATOGRAPHY A

www.elsevier.com/locate/chroma

Axial development and radial non-uniformity of flow in packed columns

Jaekeun C. Park[a,b], Karthik Raghavan[a,b], Stephen J. Gibbs[a,b,*]

[a]*Center for Interdisciplinary Magnetic Resonance, National High Magnetic Field Laboratory, Florida State University, 1800 E. Paul Dirac Drive, Tallahassee, FL 32310, USA*

[b]*Department of Chemical Engineering, FAMU–FSU College of Engineering, 2525 Pottsdamer Street, Tallahassee, FL 32310-6046, USA*

Received 20 August 2001; received in revised form 9 November 2001; accepted 9 November 2001

Abstract

Flow inhomogeneity and axial development in low-pressure chromatographic columns have been studied by magnetic resonance imaging velocimetry. The columns studied included (a) an 11.7-mm I.D. column packed with either 50 μm diameter porous polyacrylamide, or 99 or 780 μm diameter impermeable polystyrene beads, and (b) a 5-mm I.D. column commercially packed with 10 μm polymeric beads. The packing methods included gravity settling, slurry packing, ultrasonication, and dry packing with vibration. The magnetic resonance method used averaged apparent fluid velocity over both column cross-sections and fluid displacements greater than one particle diameter and hence permits assessment of macroscopic flow non-uniformities. The results confirm that now non-uniformities induced by the conical distributor of the 11.7-mm I.D. column or the presence of voids at the column entrance relax on a length scale of the column radius. All of the 11.7-mm I.D. columns examined exhibit near wall channeling within a few particle diameters of the wall. The origins of this behavior are demonstrated by imaging of the radial dependence of the local porosity for a column packed with 780 μm beads. Columns packed with the 99-μm beads exhibit reduced flow in a region extending from ten to three-to-five particle diameters from the wall. This velocity reduction is consistent with a reduced porosity of 0.35 in this region as compared to approximately 0.43 in the bulk of the column. Ultrasonicated and dry-packed columns exhibit enhanced flow in a region located between approximately eight and 20 particle diameters from the wall. This enhancement maybe caused by packing density inhomogeneity and/or particle size segregation caused by vibration during the packing process. No significant non-uniformities on length scales of 20 μm or greater were observed in the commercially packed column packed with 10 μm particles.

Keywords: Visualization of flow inhomogeneity; Flow patterns; Packing methods; Magnetic resonance

1. Introduction

Improving the efficiency of chromatography for analytical and preparative separations has been an active research topic for decades. Considerable effort has gone into manufacturing spherical, mono-sized, porous particles to use as absorbent support material. However, relatively little systematic and fundamental knowledge concerning one of the primary causes of inefficiency, flow inhomogeneity caused by non-

*Corresponding author. Tel.: +1-850-410-6158; fax: +1-850-644-1366.

E-mail address: gibbs@magnet.fsu.edu (S.J. Gibbs).

0021-9673/02/$ – see front matter
PII: S0021-9673(01)01531-X

uniform packing density and poor flow distribution at the column entrance and exit, is in the public domain [1].

Despite decades of development in the art of column design and packing, a number of reports demonstrate that the axial mobile phase velocity is often not uniform over column cross sections [2–8]. In the present contribution, we demonstrate flow inhomogeneity caused by both packing inhomogeneity and poor flow distribution at the column entrance in columns packed with three different materials by magnetic resonance imaging velocimetry (MRIV). We find qualitatively different behavior for each of the three packing materials characterized by different particle diameter to column diameter ratios and different packing particle rigidity, although similar packing methods were used.

Although the importance of packing homogeneity in chromatographic columns has been well recognized, few experimental tools have been available to unambiguously probe packing density and fluid flow in optically opaque media. Magnetic resonance techniques are applicable to many opaque systems and allow measurement of displacements over time scales ranging from a few milliseconds to a few seconds. Measurements over these short time scales are useful for characterizing flow inhomogeneity without the confounding effects of transverse dispersion. Several applications of MRI to the study of transport in porous media have appeared recently [9–22]. Many of these studies are based on the pulsed field gradient (PFG) technique, in which it is possible to measure the spectrum of molecular displacements (or propagator) over an evolution time (or observation time) of milliseconds to seconds. These displacement spectra may be analyzed to help understand details of the convective dispersion process [21–24]. Magnetic resonance imaging (MRI), combined with PFG NMR techniques, permits measurement of the spatial dependence of fluid velocity over short time scales and observation of the development of dispersion over longer time scales in chromatographic columns. The present work focuses on long time scales for which fluid displacements are much greater than one particle diameter and for which the displacement spectra or propagators are Gaussian. These conditions are useful for assessing systematic flow non-uniformities over length scales greater than one particle diameter.

Five types of inhomogeneities are considered here: (1) random variations in packing density; (2) axial variations in packing density; (3) distributor induced flow inhomogeneities at the column entrance and exit; (4) systematic radial deviation in packing density in the immediate vicinity of the wall (i.e. within a few particle diameters of the wall); and (5) systematic radial deviation in packing density in the bulk of the column. Random fluctuations in the column packing density will always be present in columns formed from particulates. One goal of consolidating the packing is to eliminate fluctuations on length scales larger than a few particle diameters. Column compression, vibration, and ultrasonication have been employed to consolidate the packing with varied results [25,26]. These random fluctuations will not be considered further in this paper. Rather, we focus on the macroscopic effects, which can severely degrade column efficiency.

Axial variations in packing density may very well occur as a result of the non-uniform axial stress [27], but these have little effect on chromatographic efficiency. These variations are of interest here because the MRIV techniques can monitor changes in interstitial velocity as a function of axial position for impermeable packings, and hence allow inference of axial variation in packing density.

The flow distributors at the entrance and exit of a column should ideally provide (1) equal transit times from the inlet tubing to all points over the column cross section (or, conversely from the column cross section to the outlet tubing) and (2) equal entrance/exit fluid velocities over the column cross sections [27]. If the column is packed uniformly, then these two criteria will ensure that all streamlines through the column have identical residence times. However, columns may often not be packed uniformly, especially at the column entrance where secondary consolidation can result in the formation of void spaces. The effects of non-ideal distributor design have been investigated theoretically [27] and experimentally [28]. Dimensional analysis and numerical calculations of flow development in porous media following Darcy's law and with uniform permeability indicate development lengths scale with the column diameter. Hence, these effects can be very

important for short, wide columns. The photographs of band development presented in [28] show clear evidence of non-uniform entrance residence times over the column cross-section; unambiguous analysis of these data is made difficult by the confounding effects of possible flow non-uniformity over the column cross section.

Packing heterogeneity in the near wall region is perhaps easiest to understand. Because of steric exclusion of particles from the wall and because of wall-induced ordering of particles in the immediate vicinity of the wall, it is expected that the void fraction in the immediate wall vicinity may be substantially larger than in the bulk of the column. We refer to this phenomenon as ''wall channeling''. Du Plessis and Roos [29] numerically simulated wall channeling considering a local bed void fraction $\epsilon(y)$ which decreases with increasing distance y from the wall as $\epsilon(y) = \epsilon_b[1 + \exp(-2y/d_p)]$, where d_p is the particle diameter. Sederman and co-workers [14,16] have measured the instantaneous local velocities in pores of packed beds of impermeable particles and have found significant flow enhancement in pores within one or two particle diameters of the wall. Sharma et al. [20] have measured voidage distributions in packed beds of large particles with high resolution MRI and found the expected increased voidage within one particle diameter of the wall and oscillatory relaxation to near random packing after approximately three particle diameters from the wall [30,31]. Shalliker et al. [7] have recently reported spatially resolved optical measurements of fluid velocity and column efficiency. They found that in the immediate wall region, fluid velocity is substantially larger and that the column efficiency is substantially less than in the bulk of the column. Harding and Baumann [32] have observed significant near wall channeling in columns packed with an agarose-based gel. Previous studies using MRI for columns packed with small chromatographic particles [33] have not had sufficient spatial resolution to observe this ''wall channeling'', although the radically compressed columns used in that study may not exhibit significant channeling. Our own previous study [6] indicated significant wall channeling but did not address axial development of flow.

The ''far wall'' region extending from approximately 5 to 30 particle diameters from the wall is more complex; experimental observations of bed inhomogeneity seem to depend upon the packing method employed. Knox et al. [2] and Eon [34] investigated columns packed with glass beads using dry packing methods by using radically localized tracer injection and detection and found that flow was faster in a band extending approximately 30 particle diameters from the column wall than near the center of the column. Conversely, several other investigations [3–5,8] (and references contained therein) have found for slurry packed columns that flow is significantly slower in a region within some tens of particle diameters of the wall. Farkas et al. [3] have attributed these two different behaviors to the differences in packing methods employed. Shalliker et al. [7] demonstrated a substantially reduced fluid velocity in the far wall region for slurry packed columns of silica. Our own previous work using MRI [6] showed significantly reduced fluid velocity in the far wall region, but we could not rule out effects of the inlet distributor. Harding and Baumann [32], using MRI, have observed velocity reduction in the far wall region in columns packed with agarose-based gel. Other investigations of radially compressed slurry packed columns have shown no significant deviations in the far wall region [33]. The origins of these differing behaviors are not clear at present, although slower flow in the far wall region has been attributed to non-uniform packing stress caused by axial compression and wall friction [26].

The present work seeks to clarify this situation by examining systematic radial variations in axial fluid flow in columns packed with different materials and packing methods. The methods employed measure fluid velocities averaged over slice thickness and fluid displacements greater than one particle diameter in order to focus on macroscopic inhomogeneities of severe consequence for column efficiency.

2. Experimental

2.1. Column preparation

Acrylic columns of 11.7 mm I.D. (BioSepra, Marlborough, MA, USA, now Life Technologies, Rockville, MD, USA) were packed with either 99

μm average particle diameter polystyrene beads (Bangs Labs., Fishers, IN, USA); 780 μm average particle diameter polystyrene beads (Bangs Labs.); or 50 μm average particle diameter polyacrylamide size-exclusion beads (BioSepra, now Life Technologies, Rockville, MD, USA). The particle size distributions (±one standard deviation) are claimed by the manufacturers to be 90–106 and 710–850 μm, respectively, for the polystyrene beads, and 40–80 μm for the polyacrylamide beads.

A piston pump Model ACCU FM-50 with RH00 head (SciLog, Madison, WI, USA) provides flow and was fitted with a pulsation dampener because of the extreme sensitivity of the MRI measurement technique to flow instabilities. Flow rates were measured by at least three timed collections of the column effluent. The maximum operating pressure used for the 11.7-mm column was 29 p.s.i.g. (1 p.s.i. = 6894.76 Pa).

Several column packing methods were employed:

(1) A gravity-settling from slurry packing method was tested for all packing materials. Before packing each column, the 99- and 780-μm polystyrene beads were immersed in water containing 0.005% of the surfactant, Triton X-100 (Sigma, St. Louis, MO, USA) in order to thoroughly wet the bead surfaces and a small amount of bacteriostat, Sigma Clean water bath treatment for 1 day.

The columns were packed by gravity settling of an aqueous suspension of beads. The entrance distributor was then replaced and the bed slightly axially compressed by 2–3 mm in order to remove air voids near the top of the column, which were difficult to completely avoid. In each case the bed packing length was about 6 cm. A schematic of the distributor geometry is shown in Fig. 1.

(2) A low-pressure slurry packing method was tested for columns packed with the 99- and 50-μm beads. In this method, suspensions of the appropriate packing material (as described above) were forced into the column at 29 p.s.i.g.

(3) The gravity-settling from slurry packing method was performed as above for the 99-μm particles in an ultrasonic bath (Model 2510, Branson, CT, USA). After finishing packing, the columns were exposed to ultrasound for an additional 2 h.

(4) A dry packing method was tested with the 99- and 780-μm beads. In this method, a motor-driven cam continuously vibrated the column vertically at a speed of 270 rpm with a displacement amplitude of 5 mm. The packing material was fed into the column as a continuous fine stream. After finishing packing, the columns were allowed to vibrate vertically for 1 h. The entrance distributor was then fitted.

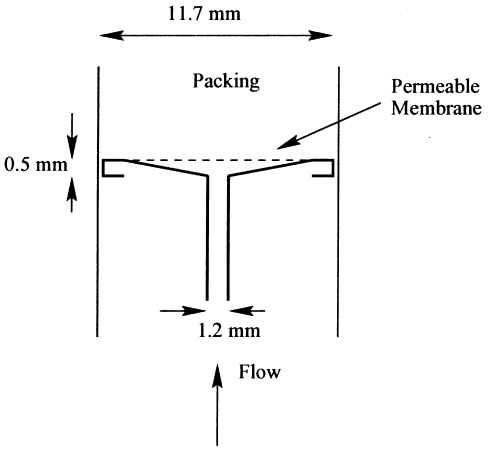

Fig. 1. Schematic of the flow distributor used.

Further consolidation of each column for all packing methods was achieved by flow of degassed water through the column for 10–12 h at 29 p.s.i.g. After this period, the entrance distributor was again adjusted by 1–2 mm for the 50- and 99-μm columns.

We also investigated a commercially packed column with 10 μm polymeric beads (Mono Q, HR 5/5, Amersham Pharmacia Biotech, Piscataway, NJ, USA). An HPLC pump (series IV, Fisher Scientific, Pittsburgh, PA, USA) was used to pump deionized, degassed water through the column. Flow rates were determined by timed collection.

2.2. MRI methods

Measurements described herein were performed with a Bruker Avance DRX spectrometer operating at 500 MHz for protons and coupled with an 11.7-T, 89 mm bore magnet or with a Bruker Avance DMX spectrometer operating at 600 MHz for protons and coupled with a 14-T, 89 mm bore magnet. These systems are both equipped with an actively shielded gradient set capable of switching 0.96 T/m in 110 μs at 40 A. Each column was placed in a 15-mm I.D. (or 25 mm I.D. in the case of the Mono Q column)

''bird cage'' type radio-frequency probe (transmitter–receiver coil length, approximately 4.3 cm) and inserted into the bore of magnet.

The MRI pulse sequence for velocity imaging employed in our work is shown in Fig. 2. The first part of the sequence is a 13-interval alternating pulsed gradient stimulated echo (APGSTE) sequence used for motion encoding [35]. Magnetization encoded in this fashion is then stored longitudinally for later readout by a slice-selective spin–warp spin–echo sequence used to obtain spatially resolved data [36]. The slice selective pulses used were either 1-ms 3-lobed $\sin(x)/x$ pulses or 1-ms ''pre-focussed'' pulses [37,38]. The phase cycling used for the imaging study is a 32-element cycle designed to eliminate unwanted echoes and signal resulting from longitudinal relaxation during the storage periods. The APGSTE sequence encodes displacement in the phase of the nuclear magnetization so that if the spectrum of displacements (or localized propagator) is Gaussian, then the local nuclear magnetization is described by:

$$S(\mathbf{r}) \approx S_0(\mathbf{r}) \exp(-q^2 \mathcal{D}(\mathbf{r})\Delta) \exp(-i\mathbf{q} \cdot \mathbf{v}(\mathbf{r})\Delta) \quad (1)$$

Where $S(\mathbf{r})$ is the measured signal proportional to the local nuclear magnetization, $S_0(\mathbf{r})$ is a normalizing factor proportional to the local nuclear magnetization in the absence of motion encoding, $\mathbf{q} = \gamma\delta\mathbf{g}$, γ is the magnetogyric ratio of the nucleus being observed, δ is the duration of the motion encoding magnetic field gradient pulses, $\mathcal{D}$ is the effective dispersion coefficient in the direction of the motion encoding gradient pulses, Δ is the time interval between motion encoding gradient pulses during which displacement occurs, and $v(\mathbf{r})$ is the local velocity.

After placing each column in the radio-frequency coil and in the magnet, flow was re-established and a

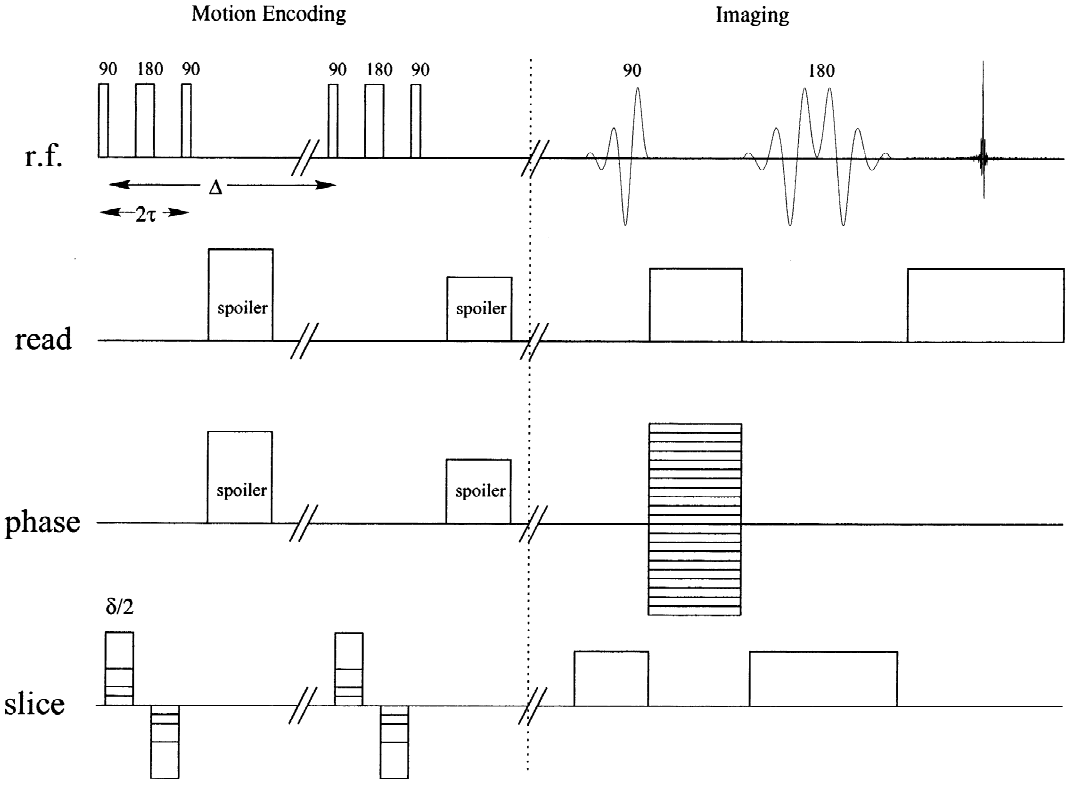

Fig. 2. Timing diagram for the NMR 13-interval alternating pulsed gradient stimulated echo (APGSTE) imaging pulse sequence. Shown are timelines for events on the radiofrequency (r.f.) and read, phase, and slice magnetic field gradient channels.

pilot MRI image was obtained vertically through the column. This image was used to establish the locations of transverse slices through the column for examination by velocity imaging. For the column packed with 780 μm beads, four slices each of thickness 3 mm and separated by 1 mm were taken. For the 99- and 50-μm bead column six slices of thickness 2 mm and separation 1 mm were taken. For each of the slices, approximately ten 128×128 pixel images over a 1.4-cm field of view were acquired corresponding to ten different values of the motion encoding magnetic field gradient pulse **g**, which was always oriented along the axis of the column in the flow direction. For the Pharmacia column, the field of view was 0.7 cm. The value of Δ was chosen to be long enough such that the fluid travels at least one particle diameter during this time; for these conditions, the propagator is approximately Gaussian and Eq. (1) is valid. Data at each location of the image were then analyzed by maximization of the generalized Lomb–Scargle periodogram [39,40] to obtain estimates of the local axial velocity.

2.3. Spatial variation in packing density

From the velocimetry data it is possible to estimate spatial variations in packing density under certain assumptions. Axial variations in the cross-sectionally averaged packing density can be directly inferred from axial variations in the cross-sectionally averaged fluid velocity by $\epsilon = Q/(Av_a)$, where ϵ is the total porosity, Q is the volumetric flow-rate obtained from timed collection, and v_a is the cross-sectionally averaged velocity. For impermeable particles, the porosity measurement is straightforward, but for porous particles the porosity obtained is a combination of intra- and interparticle porosity.

For flows in which the axial pressure gradient is independent of radial position (e.g. fully developed flow in which the only permeability variation is in the radial direction), the radial variation of the relative Darcy permeability may be obtained from radial variation in the fluid velocity. Then, using the constraint that the cross-sectionally averaged porosity is already known from above and assuming that the local average particle size is independent of radial position, the radial variation in porosity can be obtained in an iterative calculation. Specifically, it is first assumed that Darcy's law:

$$v = -\epsilon^{-1}\mu^{-1}\mathbf{K}\cdot\nabla P \tag{2}$$

applies. The factor of ϵ^{-1} on the right hand side comes from the fact that the velocity on the left hand side is the interstitial velocity measured by velocimetry as opposed to the Darcian velocity based on the column cross-sectional area. Then it is assumed that $\nabla P = \mathrm{d}P/\mathrm{d}z$ and is independent of radial position. Then the local permeability is assumed to be given by the Carman–Kozeny expression [41] $K = d_p^2\epsilon^3/[180(1-\epsilon)^2]$ where d_p is the particle diameter. Therefore, macroscopic (over more than a few particle diameters) variations in the local velocity can be described by:

$$v(r) = \alpha\epsilon(r)^2/[1-\epsilon(r)]^2 \tag{3}$$

where α is an unknown constant representing the local axial pressure drop and other void-fraction independent factors. The calculation of the radial variation in permeability then proceeds by finding a value of α for which the cross-sectionally averaged porosity computed by solving Eq. (3) using the measured radial velocity distribution corresponds to that determined from the cross-sectionally averaged velocity, cross-sectional area, and volumetric flow-rate.

This procedure only applies to impermeable particles for which the interparticle porosity can be obtained by the method in the preceding paragraph. Hence for our work, it is only applicable to fully developed, Darcian flow in the 99-μm bead columns. For beds packed with small porous particles, the interparticle porosity is not known; for beds packed with large particles (i.e. the 780-μm beads in which the column-to-bead diameter ratio is only 15) Darcy's law does not effectively describe spatial variations in fluid velocity.

For beds of larger particles (i.e. the 780-μm particles in our studies), particle sizes and positions can be determined directly from high-resolution MR images as has been done by Sharma et al. [20]. These data can then also be used to calculate radial and axial variations in the column porosity. In order to do so for our non-porous particles, a high-resolution three-dimensional image collected by stan-

dard methods is first thresholded at a level of one half the intensity of the fluid-filled regions; regions having an intensity above this level are assigned a value of unity and regions falling below this level are assigned a value of zero. Axial and azimuthal averages of the resulting image then yield axial and azimuthal variations in the void fraction. The measurements thus obtained are sensitive to the exact level of the threshold used and to spatial variations in the MR coil sensitivity. The latter concern can be addressed by obtaining a map of coil sensitivity on a uniform sample and using it to correct the image intensities. For our instrumentation, variations in image intensity on a uniform sample are on the order of 10%, and we have not yet pursued such corrections.

Extensions of the above approach based on image signal intensity to small particles for which one image pixel contains many particles are possible. However, since very small changes in the void fraction can result in large changes in the permeability, signal-to-noise ratios of at least 100:1 in the image measurements would be necessary in order to resolve significant variations in porosity. Our typical signal-to-noise ratios are on the order of 10:1. Furthermore, interpretation of signal intensities for images of columns packed with small particles is confounded by differential T_2 nuclear relaxation as a function of void fraction. This difficulty could be partially alleviated by acquiring a series of images with different effective echo times and extrapolating to zero echo time in order to obtain better estimates of the true local magnetization or fluid density.

3. Results and discussion

We organize the discussion of our results by first presenting in detail a discussion of the results for the gravity-settling packing method. These results then serve as a basis of comparison for the other columns and packing methods studied. The results for all columns presented here are summarized in Table 1. These results are qualitatively representative of the flow phenomena observed for each packing material and packing method.

3.1. The gravity-settling packing method

For the three types of column packings studied, we have studied several repetitions of the gravity-settling packing process. For the 50-μm polyacrylamide we have repeated the packing process four times, for the 99-μm polystyrene four times, and for the 780-μm polystyrene twice. For fully developed flow, each packing material exhibits a

Table 1
Radically averaged velocities/apparent void fractions

Column	Radically averaged velocity (cm/s)/apparent void fraction								
	780 μm		99 μm				50 μm		Mono Q 10 μm
	GS	Dry	GS	LP	US	Dry	GS	LP	
Slice 1	0.40/0.57	0.358/0.48	0.291/0.39	0.310/0.38	0.264/0.57	0.254/0.56	0.0151/0.93	0.0154/0.90	0.0837/1.02
Slice 2	0.53/0.43	0.386/0.45	0.306/0.37	0.290/0.40	0.377/0.40	0.432/0.33	0.0154/0.91	0.0152/0.91	0.0946/0.91
Slice 3	0.56/0.41	0.401/0.43	0.284/0.40	0.293/0.40	0.367/0.41	0.360/0.40	0.0156/0.90	0.0143/0.97	0.0938/0.92
Slice 4	0.53/0.43	0.387/0.45	0.281/0.40	0.29/0.40	0.364/0.41	0.353/0.41	0.0140/0.99	0.0152/0.91	0.0942/0.92
Slice 5			0.284/0.40	0.313/0.37	0.363/0.41	0.351/0.41	0.0144/0.97	0.0152/0.91	0.0914/0.94
Slice 6			0.282/0.40		0.365/0.41	0.348/0.41	0.0149/0.94	0.0158/0.88	
Average velocity (cm/s)	0.51±0.07	0.383±0.01	0.288±0.009	0.299±0.004	0.365/0.41±0.004	0.350±0.023	0.0149±0.0006	0.0152±0.002	0.0917±0.005
$\epsilon_{average}$	0.45	0.45	0.395	0.39	0.41	0.41	0.94	0.91	0.94
Re_i	3.97	2.98	0.28	0.30	0.36	0.35	0.007	0.008	0.009
$v\Delta/d_p$	1.3	1.5	9.0	9.3	11.3	10.8	3.0	3.0	9.5

GS, gravity settled; Dry, dry packed with vibration; LP, slurry packed; US, slurry packed with ultrasonication; $v\Delta/d_p$, number of particle diameters that the fluid travels during the measurement interval Δ; Re_i, interstitial Reynolds number.

characteristic behavior. The entrance flow depends more upon the distributor and the presence of any voids at the column entrance. We present below in detail the results for three representative columns showing behavior characteristic of the three materials.

Fig. 3 shows a longitudinal image through the 11.7-mm I.D. column packed with 50 μm beads. Also indicated on the left are the positions of the six slices interrogated for this column. Also seen is the geometry of the flow distributor.

Fig. 4 shows radial profiles of the axial velocity obtained from the MRIV data for the six different slices in the column packed with the 50-μm polyacrylamide size-exclusion beads. These radial profiles were obtained from the cross-sectional velocity maps by methods already described in our previous work [6]. Note that several important details of the procedure for going from the two-dimensional Cartesian map to a radial plot are discussed in Ref. [42]. The spatial resolution in these azimuthally averaged radial plots depends not upon the voxel size but rather upon the precision with which the center of the column can be identified and the degree to which the column cross section deviates from a perfect circle. A series of caliper measurements of the 11.7-mm column internal diameter had a standard deviation of 40 μm; we expect this to correspond roughly to the effective spatial resolution the radial plots. The cross sectional velocity maps were inspected for approximate axial symmetry before further analysis. Figs. 5 and 6 show similar data for columns packed with the 99- and 780-μm polystyrene beads, respec-

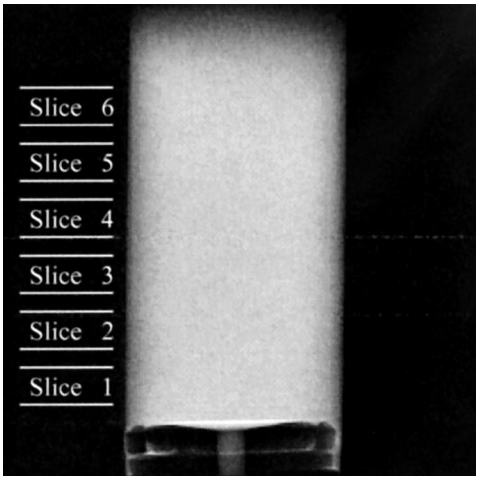

Fig. 3. MR image of the slice positions in column packed with porous 50 μm diameter polyacrylamide size-exclusion beads.

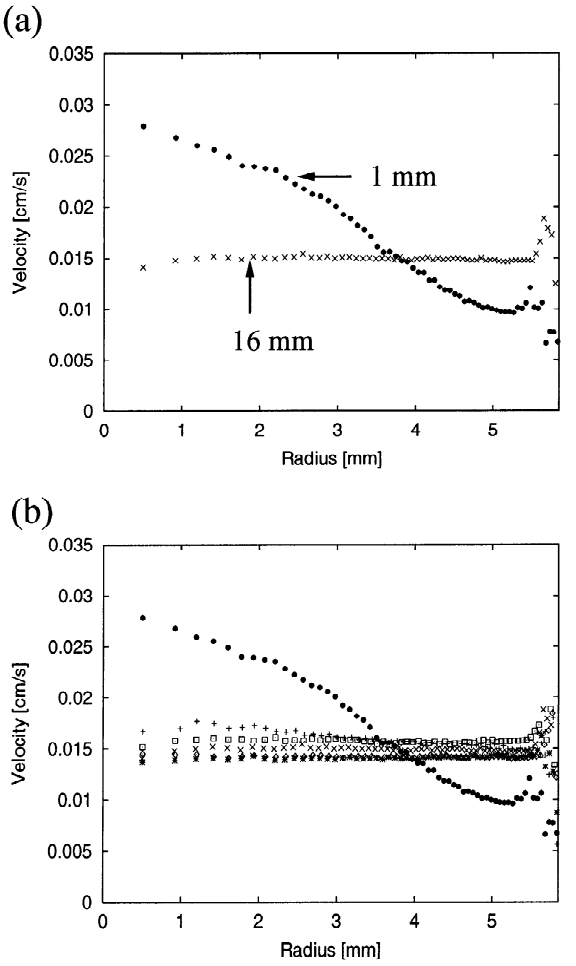

Fig. 4. Radial fields of axial velocity showing flow development in the column packed with porous 50 μm diameter polyacrylamide size-exclusion beads. The evolution time, Δ, is 1005 ms. Each slice thickness is 2 mm and the slices are separated by 1 mm. (a) The axial velocity fields in the slice closest to (1 mm) and farthest (16 mm) from the entrance distributor. (b) All slices. Points represent the average of axial velocities in 200 pixels within a given radial bin. The standard deviation in each bin is approximately ±10% of the velocity. The distance of the slices from the entrance distributor are: ●=1 mm; +=4 mm; □=7 mm; *=10 mm; ◇=13 mm; ×=16 mm. The overall flow-rate is 0.015 ml/s.

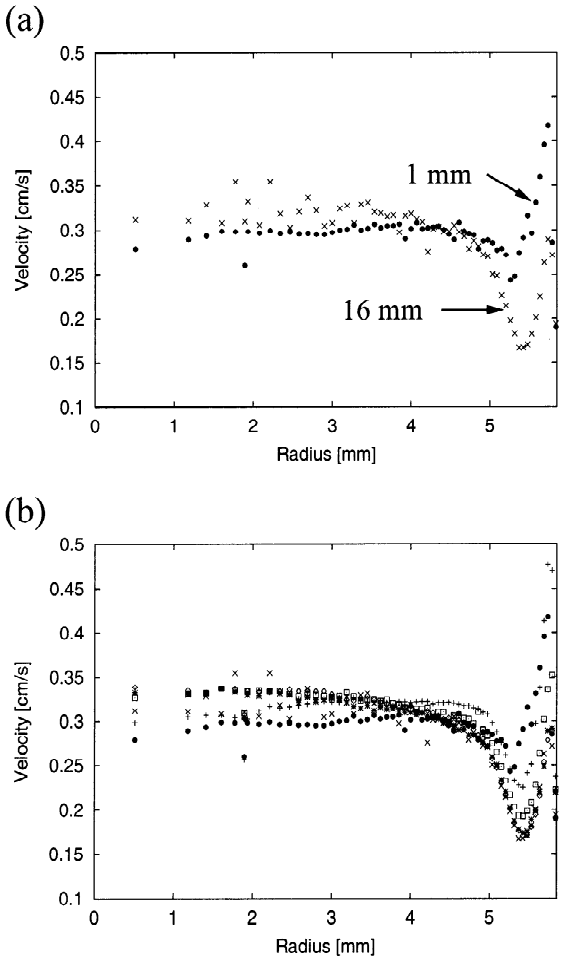

Fig. 5. Radial fields of axial velocity showing flow development in a column packed with impermeable 99 μm diameter polystyrene beads. The evolution time, Δ, is 308 ms. Each slice thickness is 2 mm and the slices are separated by 1 mm. (a) The axial velocity fields in the slice closest to (1 mm) and farthest from (16 mm) the entrance distributor. (b) All slices. Points represent the average of axial velocities in 200 pixels within a given radial bin. The standard deviation within each bin is approximately 10% of the velocity. The distance of the slices from the entrance distributor are: ●=1 mm; +=4 mm; □=7 mm; *=10 mm; ◇=13 mm; ×=16 mm. The overall flow-rate is 0.12 ml/s.

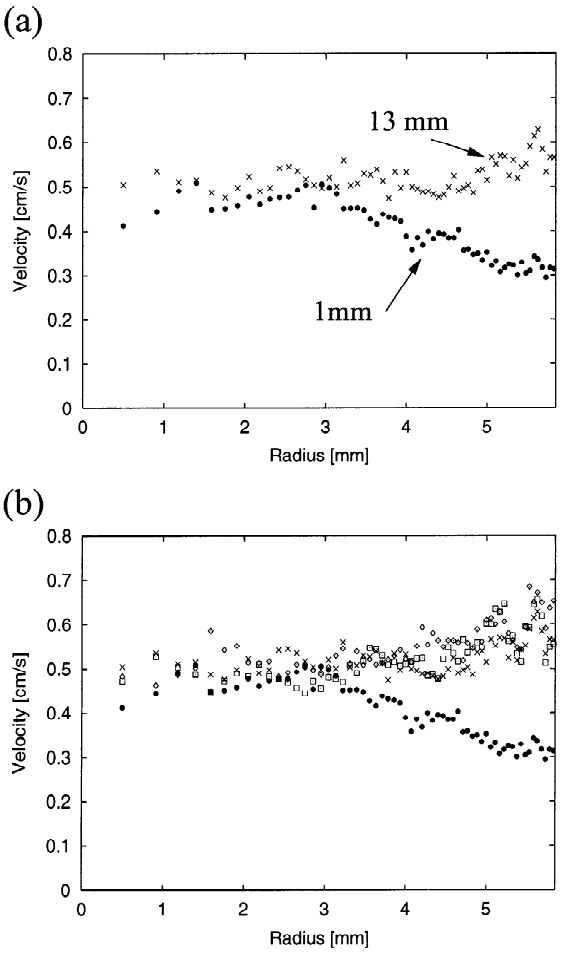

Fig. 6. Radial fields of axial velocity showing flow development in the column packed with impermeable 780 μm diameter polystyrene beads. The evolution time, Δ, is 205 ms. Each slice thickness is 3 mm and the slices are separated by 1 mm. (a) The axial velocity fields in the slice closest to (1 mm) and farthest from (13 mm) the entrance distributor. (b) All slices. Points represent the average of axial velocities in 200 pixels within a given radial bin. The standard deviation in each bin is approximately 40% of the mean. The distance of the slices from the entrance distributor are ●=1 mm; □=5 mm; ◇=9 mm; ×=12 mm. The overall flow-rate is 0.26 ml/s.

tively. The velocity profiles have some common features, but behavior in columns packed with different materials is qualitatively different.

Before examining the three data sets in detail, we check the consistency of the data by computing the cross-sectional averaged velocity for each slice (weighted by radial position) and by calculating an apparent column void fraction from the interstitial velocity and the volumetric flow-rate obtained by timed collection. Table 1 shows the average velocities for all slices in each of the three data sets. The

average velocities should be the same for each slice in order to satisfy a material balance if the bed void fraction does not depend upon axial position; for the two smaller bead columns the inter-slice standard deviation is less than 5%. This order of magnitude of variation is typical of MRI data and can be attributed in part to spatial variation in the applied magnetic field gradients for motion encoding. For the 780-μm bead column, however, the first slice has a substantially lower velocity than the other slices. This may in part be due to the presence of a void within this slice, but another explanation for this deviation is related to the much faster flow in this column of larger beads. For all of our flow measurements, the time interval for motion encoding Δ was chosen so that fluid moves at least one particle diameter during this interval. For the large particle column, this distance is comparable to the distance between the distributor and the leading edge of the first slice. During the time interval for motion encoding, fresh fluid enters the slice that has not been excited by the radio frequency pulses during the first part of the MRI pulse sequence. Therefore, little signal is obtained from the fast moving regions and the resulting velocity is underestimated in the fast moving area near the center of the column. This effect could be avoided by placing a fluid reservoir inside the radio-frequency coil just prior to the distributor in the flow path.

The average void fractions calculated for each column are reasonable. The 99-μm bead column has a void fraction of 0.4, consistent with random packing of impermeable particles. The 780-μm bead column has a slightly larger void fraction possibly resulting from the larger bead to column diameter ratio. The apparent void fraction for the 50-μm bead column is nearly unity, suggesting that water has nearly complete access to the pore spaces of the polyacrylamide gel particles.

3.1.1. Flow development

The results for all columns studied show that flow is nearly fully developed at a distance of about 6 mm or one column radius from the entrance distributor, but each column shows different entrance behavior. The entry flow profile for the 780-μm columns studied may be unreliable for the reasons described above, but are qualitatively similar to the entry profiles for the 50-μm columns. These entry profiles are consistent with the solute band development images recently reported by Harding and Baumann [32] for a similar distributor geometry. The entry profile for the 99-μm column presented here is very different because of the presence of packing voids at the column entrance. Fig. 7 shows axial images through the distributor region for a column packed with each material. Image (b) for the 99-μm bead column shows a water-filled void space in the column below the distributor. For the other two

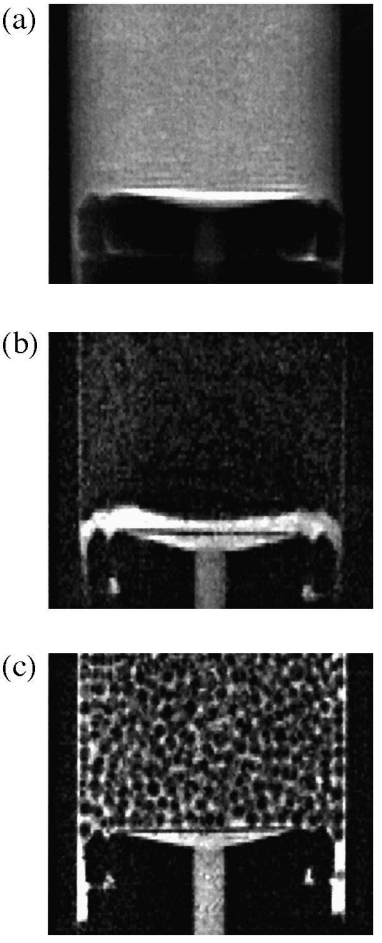

Fig. 7. MR image of the inlet distributor and column entry region for the column packed with (a) 50 μm permeable polyacrylamide beads, (b) impermeable 99 μm diameter polystyrene beads, and (c) 780 μm polystyrene beads. Note that there is a convex void at the entrance of the 99-μm bead column. Also note the particle ordering near the wall for the 780-μm bead column.

columns there is no such void space. Furthermore, for the 99-μm bead column, packing in the central region of the column is closer to the distributor, perhaps because the packing had been moulded by the conical distributor prior to secondary consolidation. These differences are consistent with slower flow in the central entry region of the 99-μm column with a void space present than in other columns. In all cases studied, flow development is complete, within our experimental resolution, within approximately one column radius (6 mm) of the entrance distributor.

The calculations of Yuan et al. [27] and the experimental evidence of Broyles et al. [28] suggest that a sudden expansion distributor consisting of a small diameter inlet tube and a porous frit of diameter to match the internal diameter of the column, provides adequate uniformity in the exit velocity from the distributor. Our experimental evidence suggests that the conical distributor provides poorer flow homogeneity than the sudden expansion or the improved designs proposed by Yuan et al. [27].

3.1.2. Near wall channeling

The fully developed flow profiles in all columns studied are consistent with a significant near wall channeling effect. Axial velocities are largest in a region within five particle diameters of the wall. For all columns, the axial velocity begins to decrease as the wall is very closely approached consistent with no slip at the wall surface. For the 780-μm bead column, the radial spatial resolution is sufficient to show the effects of particle ordering near the wall; in the two intermediate velocity profiles shown in Fig. 6b, peaks are present in the velocity profiles at a distance of approximately one particle diameter from the wall and at approximately 1/5 of a particle diameter from the wall. Our examination of the 780-μm columns is also significantly different from the other two columns in that ratios of slice thickness to particle diameters are larger than 20 for the small bead columns and is less than 4 for the 780-μm bead columns; also the ratio of average fluid displacement to particle diameter is less (see Table 1). These factors may cause significant variation in the apparent velocity even after azimuthal averaging.

The thickness of the wall channeling region observed here is larger than that predicted from observed porosity variations [29] by approximately a factor of two. Incomplete particle consolidation near the wall and Brinkman effects [41] could cause this thicker wall channeling region.

3.1.3. The far wall region

The radial profiles of axial velocity in the 99-μm bead column show a region of significantly decreased velocity in the vicinity of 10–5 particle diameters from the wall. The velocity reduction is dramatic, on the order of a factor of 2, but could easily be caused by systematic radial variations in the packing void fraction. We have observed this effect reproducibly in other columns packed with the same particles and have now demonstrated that it is not caused by the flow distributor. Shalliker et al. [7] have recently demonstrated similar behavior by monitoring sample band migration in a column slurry packed with YMC C_{18} silica. They observed both the near wall channeling and the far wall flow reduction, but did not definitively eliminate effects of the flow distributor. Our results show a larger radial velocity variation; the small variation observed by Shalliker et al. [7] may be due in part to radial smoothing of the actual velocity profile by transverse dispersion over the longer length and time scales used for those optical measurements.

The origin of the far wall velocity reduction has been supposed to be due to wall friction increasing the compressive stress and hence the packing density during the packing and consolidation process near the wall [2,7,27,34,43,44].

3.1.4. Spatial variation in void fraction

The axial variations in packing density have been summarized in Table 1. All of these values are within expected ranges except for the first slice of the 780-μm column and the first slices of the vibrated 99-μm columns (discussed below). The value for the 780-μm bead column may be in error for the reasons discussed above. These large values would also be consistent with the presence of voids at the column entrance.

We performed the trial-and-error void fraction calculation on the fully developed velocity profile for the 99-μm bead column shown in Fig. 5; the resulting radial void fraction distribution is shown in

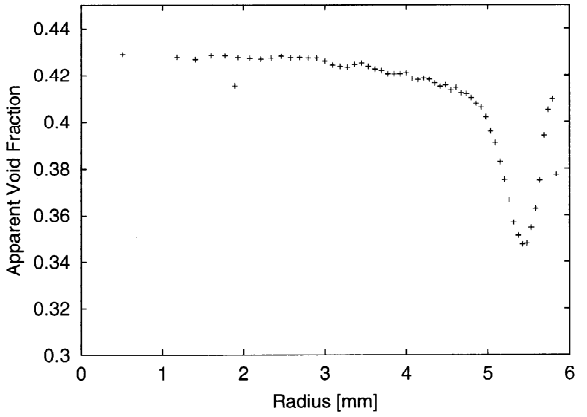

Fig. 8. Apparent radial void fraction variation in a 99-μm bead column packed by gravity settling. The void fraction distribution is calculated by assuming potential flow, a pressure gradient independent of radial position far from the distributor,an average particle size independent of radial position, and the Carman–Kozeny dependence of permeability upon local void fraction.

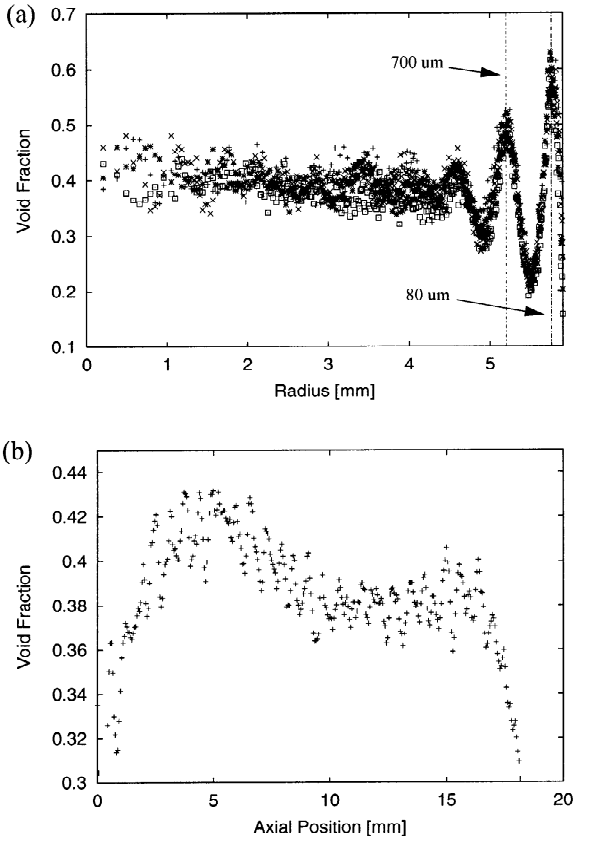

Fig. 9. Radial (a) and axial (b) void fraction distributions in a 780-μm bead column. The distributions were determined by 3-dimensional MRI followed by thresholding and spatial averaging. The radial profiles correspond to averages over 25 contiguous slices through the column cross section spanning 1.4 mm; each symbol represents a different 1.4 mm section and shows nearly identical behavior independent of axial position. The fact that the void fraction does not approach unity at the column radius is an artifact of the measurement technique resulting from a finite voxel size of 55×55×55 μm. The artifact peak occurs at a distance of 80 μm from the wall and the next peak occurs at a distance of 700 μm from the wall. The axial profile corresponds to averages over the entire column cross section for different axial positions from the distributor located at an axial position of 0 mm.

Fig. 8. The local void fraction varies from a minimum of 0.35 to a maximum of 0.43. This range of variation is certainly possible; rhombohedral packing has a void fraction of 0.26 and cubic packing has a void fraction of 0.47. However, the calculations are based on the assumptions that dP/dz is independent of r far from the column ends and that there is no spatial segregation in particle sizes. In order to account for the factor of two variation in local velocity, the ratio of local particle sizes at the column center to the region of minimum velocity would have to be approximately 1.5. This value is substantially larger than the manufacturer's specific cations of the distribution of particle sizes.

We also performed high-resolution three-dimensional imaging of a 780-μm column packed by the gravity settling method. The image was acquired with a spin–echo sequence [36] in a 512×256×256 matrix over a 2.8×1.4×1.4 cm field of view for an isotropic spatial resolution of 55 μm. The image was thresholded and processed as described above to obtain the axial and radial porosity profiles shown in Fig. 9. The average value of the porosity is sensitive to the value of the threshold used but the pattern of spatial variations is not. The plot of porosity versus radial position shows the expected oscillation in apparent void fraction as the wall is approached; a peak occurs at a distance of 700 μm from the wall in good agreement with the expected peak at one particle diameter from the wall [20,30,31,45–47]. The porosity decrease within 100 μm of the wall is an artifact of the finite voxel size in the image; for

infinitesimal voxels, the porosity should approach unity at the wall. The axial plot shows a steep increase from the entrance of the column with a value of 0.32 to a value of 0.42 and then a gradual decrease to 0.38 at a distance of 10 mm from the entrance. The high packing density in the first millimeter from the entrance may be a result of the particles packing tightly against the flexible membrane of the distributor. This result contrasts with the porosity in the entry region determined for a similarly packed column by velocimetry (see Table 1 and the discussion at the beginning of Section 3.1).

At present we can only speculate about the origins of the differences in behavior of our 50 μm bead columns, which show no far wall velocity reduction, and the 99-μm bead columns. The 50-μm beads are porous polyacrylamide and the 99-μm beads are more rigid polystyrene. Other workers have reported uniform velocity profiles in radially compressed chromatographic columns measured by MRI [33]. Harding and Baumann [32] have recently reported NMR velocity images which demonstrate both near wall channeling and far wall velocity reduction in columns packed with gel particles. Their data suggest that the two phenomena depend upon bed consolidation, and the phenomena were least pronounced for an interparticle void fraction of 0.39. It is clearly important to understand the origins of these phenomena to improve the column packing process.

We now compare velocity profiles obtained in columns packed by other methods.

3.2. Low-pressure slurry packing

Fig. 10 shows radial profiles of the axial fluid velocity for a 99-μm polystyrene bead column packed with the low-pressure (LP) slurry method described above. The results are not significantly different from the gravity settling method; comparable near wall channeling within three particle diameters of the wall and velocity reduction between three and 10 particle diameters from the wall are observed. However, flow in the entry region differs from that in Fig. 5 because of a smaller void region in the LP column. Results for the low-pressure slurry method with the 50-μm polyacrylamide beads are nearly identical to those presented in Fig. 5 and are not presented here.

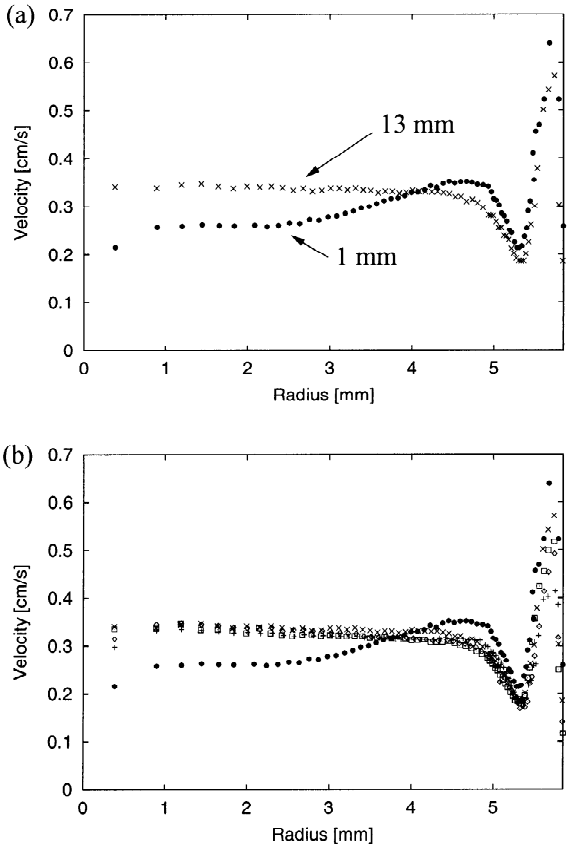

Fig. 10. Radial fields of axial velocity showing flow development in a column packed with impermeable 99-μm diameter polystyrene beads by the low pressure slurry method. The evolution time, Δ, is 308 ms. Each slice thickness is 2 mm and the slices are separated by 1 mm. (a) The axial velocity fields in the slice closest to (1 mm) and farthest from (16 mm) the entrance distributor. (b) All slices. Points represent the average of axial velocities in 200 pixels within a given radial bin. The standard deviation within each bin is approximately 10% of the velocity. The distance of the slices from the entrance distributor are: ●=1 mm; +=4 mm; □=7 mm; *=10 mm; ×=13 mm: The overall flow-rate is 0.125 ml/s.

3.3. Gravity settling with ultrasonication and dry packing with vibration

Figs. 11 and 12 show radial profiles of the axial fluid velocity for 99 μm polystyrene bead columns packed by the dry method and the gravity settling packing method in the presence of ultrasonication, respectively. These profiles show both near wall

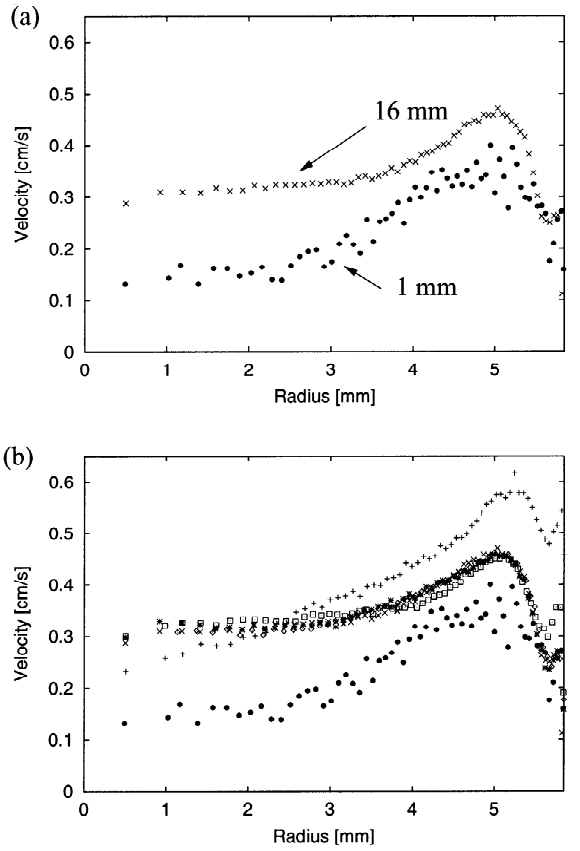

Fig. 11. Radial fields of axial velocity showing flow development in a column packed with impermeable 99 μm diameter polystyrene beads by the gravity settling method followed by ultrasonication. The evolution time, Δ, is 308 ms. Each slice thickness is 2 mm and the slices are separated by 1 mm. (a) The axial velocity fields in the slice closest to (1 mm) and farthest from (16 mm) the entrance distributor. (b) All slices. Points represent the average of axial velocities in 200 pixels within a given radial bin. The standard deviation within each bin is approximately 10% of the velocity. The distance of the slices from the entrance distributor are: ●=1 mm; +=4 mm; □=7 mm; *=10 mm; ◇=13 mm; ×=16 mm: The overall flow-rate is 0.159 ml/s.

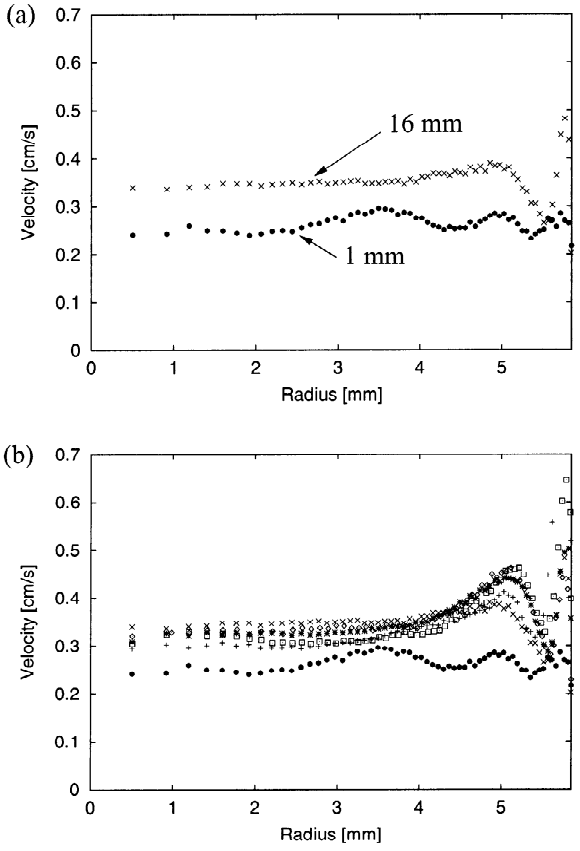

Fig. 12. Radial fields of axial velocity showing flow development in a column packed with impermeable 99 μm diameter polystyrene beads by the dry packing method. The evolution time, Δ, is 308 ms. Each slice thickness is 2 mm and the slices are separated by 1 mm. (a) The axial velocity fields in the slice closest to (1 mm) and farthest from (16 mm) the entrance distributor. (b) All slices. Points represent the average of axial velocities in 200 pixels within a given radial bin. The standard deviation within each bin is approximately 10% of the velocity. The distance of the slices from the entrance distributor are: ●=1 mm; +=4 mm; □=7 mm; *=10 mm; ◇=13 mm; ×=16 mm: The overall flow-rate is 0.155 ml/s.

channeling and far wall velocity reduction observed in the other 99-μm bead columns, but also show a region of enhanced flow just inside these regions. In addition, the entrance of the column has a substantially larger void fraction than the bulk of the column. The dry-packed column shows very similar behavior. The variation in interstitial velocity in these columns could easily be accommodated by radial variation in void fraction, but vibration during column packing and consolidation may cause radial segregation of particle sizes. The ratio of velocity in the fast flow region to that at the column center is 1.5 for the fully developed profile in the dry packed column; this could be accommodated by a corresponding ratio of particle diameters of 1.2, which is within the manufacturer's specifications of particle size variation. Vibration is known to induce particle segregation and the numerical experiments of Elperin

and Golshtein [48] suggest that larger particles migrate to the center of vibration-induced convection rolls and hence away from the container walls.

Fig. 13 shows radial profiles of the axial fluid velocity for a 780-μm bead column packed by the dry method with vibration. The entry profile is more uniform than that in the gravity settled column shown in Fig. 6. This is possibly explained by the presence of a small void at the column entrance shown in Fig. 13b similar to that shown in Fig. 5 for the 99-μm gravity settled column. In addition, the radial profiles of axial velocity exhibit significant channeling at the wall and also regions of enhanced flow at distances of one and two particle diameters from the wall which are more pronounced than observed in the gravity settled column. This may indicate increased particle ordering near the wall as a result of consolidation by vibration.

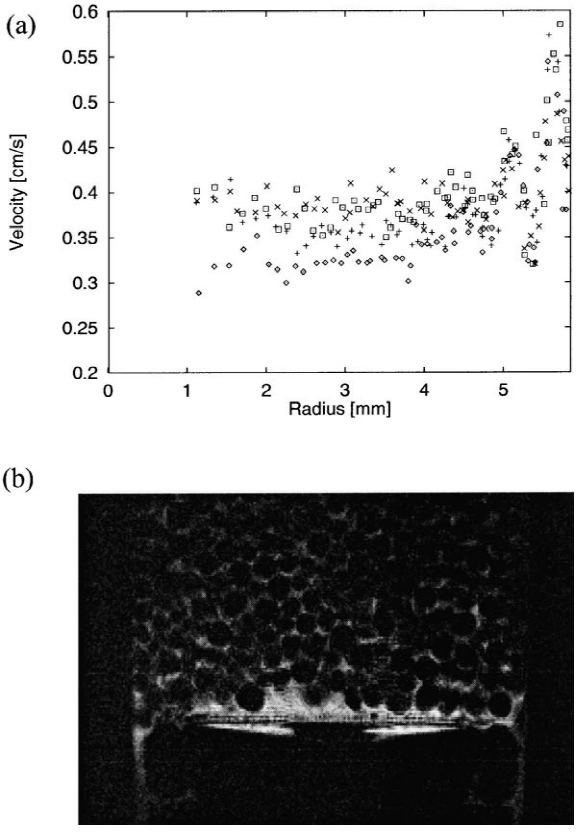

Fig. 13. Radial fields of axial velocity showing flow development in the column packed with impermeable 780 μm diameter polystyrene beads. The evolution time, Δ, is 308 ms. Each slice thickness is 3 mm and the slices are separated by 1 mm. Points represent the average of axial velocities in 200 pixels within a given radial bin. The standard deviation in each bin is approximately 40% of the mean. The distance of the slices from the entrance distributor are: ◇=1 mm; □=5 mm; +=9 mm; ×=12 mm: The overall flow-rate is 0.186 ml/s. (b) Image of the entry region of the column is showing the presence of a void. The dark region where the inlet tubing meets the distributor is caused by fast flow.

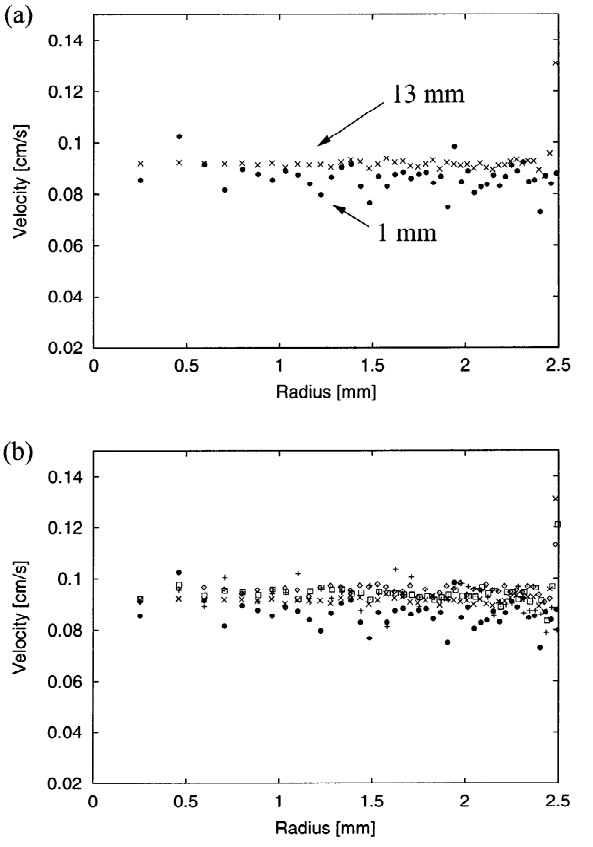

Fig. 14. Radial fields of axial velocity showing flow development in a column commercially packed with 10-μm polymeric ion-exchange beads. The evolution time, Δ, is 104 ms. Each slice thickness is 2 mm and the slices are separated by 1 mm. (a) The axial velocity fields in the slice closest to (1 mm) and farthest from (16 mm) the entrance distributor. (b) All slices. Points represent the average of axial velocities in 200 pixels within a given radial bin. The standard deviation within each bin is approximately 10% of the velocity. The distance of the slices from the entrance distributor are: ●=1 mm; +=4 mm; □=7 mm; ◇=10 mm; ×=13 mm. The overall flow-rate is 0.017 ml/s.

3.4. A commercially packed column

Fig. 14 shows radial profiles of axial velocity for flow through the Pharmacia HR5/5 Mono Q column. The profiles show that flow is nearly uniform over the column cross section for all slices studied. Our results are consistent with the presence of near wall channeling, but our spatial resolution is not sufficient to definitively characterize it.

4. Conclusions

We have measured radial profiles of the axial component of water flow in columns packed with three different materials and several packing methods as a function of distance from the inlet distributor in each column; we have also studied a commercially packed column of 10-μm polymeric beads. Each of the columns show evidence of channeling within a 3–5 particle diameters from the wall consistent with previous observations. For the columns packed in-house with a conical distributor, the flow profiles within one column radius downstream from the distributor are significantly different from the flow profiles far from the distributor. Except for near wall channeling, columns packed with the 50-μm permeable and deformable polyacrylamide beads and the column commercially packed with 10-μm beads show radially uniform velocity profiles far from the distributor. Columns packed with 99-μm polystyrene beads by either a gravity settling method or a slurry packing method, show a region of substantially decreased velocity within ten particle diameters of the wall; it is supposed that this behavior is caused by a higher packing density in this region resulting from wall friction during the packing and consolidation process. However, this ''far wall'' velocity reduction was not observed columns packed with the other materials. Columns packed with the 99-μm beads in the presence of vibration or ultrasonication, show a region of enhanced flow extending from approximately five particle diameters from the wall to about 20 particle diameters from the wall in addition to near wall channeling and region of velocity reduction within five particle diameters of the wall. This region of velocity enhancement may be caused by particle size segregation and/or a reduced packing density. These results support the notion [3] that, for some packing materials, wall friction can create a region of higher packing density and reduced permeability within 10 particle diameters from the wall and that vibration during the packing process can create a region of higher permeability within 20 particle diameters of the wall. In order to improve the performance of analytical and preparative chromatographic separations, it will be important to improve distributor function for both uniform sample injection and flow distribution, and to understand the origins and remedies for the wall effects observed.

Acknowledgements

This work was supported by the FAMU–FSU College of Engineering and the National High Magnetic Field Laboratory through the In-House Research Program supported by NSF grant DMR-9527035. The 500-MHz NMR system was acquired with funds provided by NSF grant CTS-9601924.

References

[1] J.H. Knox, J. Chromatogr. A 831 (1999) 3.
[2] J.H. Knox, G.R. Laird, P.A. Raven, J. Chromatogr. 122 (1976) 129.
[3] T. Farkas, M.J. Sepaniak, G. Guiochon, J. Chromatogr. A 740 (1996) 169.
[4] T. Farkas, G. Guiochon, Anal. Chem. 69 (1997) 4592.
[5] T. Yun, G. Guiochon, J. Chromatogr. A 760 (1997) 17.
[6] J.C. Park, S.J. Gibbs, AIChE J. 45 (1999) 655.
[7] R.A. Shalliker, B.S. Broyles, G. Guiochon, J. Chromatogr. A 888 (2000) 1.
[8] J.E. Baur, E.W. Kristensen, R.M. Wightman, Anal. Chem. 60 (1988) 2334.
[9] S. Chen, F. Qin, K.-Y. Kim, A.T. Waston, AIChE J. 39 (1993) 925.
[10] V. Rajanayagam, S.G. Yao, J.M. Pope, Magn. Reson. Imag. 13 (1995) 729.
[11] U. Tallarek, K. Albert, E. Bayer, G. Guiochon, AIChE J. 42 (1996) 3041.
[12] Y.E. Kutsovsky, L.E. Scriven, B.E. Hammer, Phys. Fluids 8 (1996) 863.
[13] Y.E. Kutsovsky, V. Alvarado, L.E. Scriven, B.E. Hammer, Magn. Reson. Imag. 14 (1996) 833.
[14] A.J. Sederman, M.L. Johns, A.S. Bramley, P. Alexander, L.F. Gladden, Chem. Eng. Sci. 52 (1997) 2239.
[15] H. Van As, D. van Dusschoten, Geoderma 80 (1997) 389.

[16] A.J. Sederman, M.L. Johns, P. Alexander, L.F. Gladden, Chem. Eng. Sci. 53 (1998) 2117.
[17] U. Tallarek, D. van Dusschoten, H. Van As, E. Bayer, G. Guiochon, J. Phys. Chem. B 102 (1998) 3486.
[18] U. Tallarek, D. van Dusschoten, H. Van As, G. Guiochon, E. Bayer, Angew. Chem., Int. Ed. Engl. 37 (1998) 1882.
[19] M.D. Mantle, A.J. Sederman, L.F. Gladden, Chem. Eng. Sci. 56 (2001) 523.
[20] S. Sharma, M.D. Mantle, L.F. Gladden, J.M. Winterbottom, Chem. Eng. Sci. 56 (2001) 587.
[21] B. Manz, P. Alexander, L.F. Gladden, Phys. Fluids 11 (1999) 259.
[22] B. Manz, L.F. Gladden, P.B. Warren, AIChE J. 45 (1999) 1845.
[23] P.T. Callaghan, Y. Xia, J. Magn. Reson. 91 (1991) 326.
[24] E. Baumeister, U. Klose, K. Albert, E. Bayer, G. Guiochon, J. Chromatogr. A 684 (1995) 321.
[25] G. Guiochon, T. Farkas, H. Guan-Sajonz, J.-H. Koh, M. Sarker, B.J. Stanley, T. Yun, J. Chromatogr. A 762 (1997) 83.
[26] R.A. Shalliker, B.S. Broyles, G. Guiochon, J. Chromatogr. A 878 (2000) 153.
[27] Q.S. Yuan, A. Rosenfeld, T.W. Root, D.J. Klingenberg, E.N. Lightfoot, J. Chromatogr. A 831 (1999) 149.
[28] B.S. Broyles, R.A. Shalliker, G. Guiochon, J. Chromatogr. A 855 (1999) 367.
[29] J.P. Du Plessis, L.I. Roos, Eng. Comp. 12 (1995) 357.
[30] R.F. Benenati, C.B. Brosilow, AIChE J. 8 (1962) 359.
[31] G.E. Mueller, Powder Technol. 77 (1993) 313.
[32] S.G. Harding, H. Baumann, J. Chromatogr. A 905 (2001) 13.
[33] U. Tallarek, E. Bayer, D. van Dusschoten, T. Scheenen, H. Van As, G. Guiochon, U.D. Neue, AIChE J. 44 (1998) 1962.
[34] C.H. Eon, J. Chromatogr. 149 (1978) 29.
[35] R.M. Cotts, M.J.R. Hoch, T. Sun, J.T. Martert, J. Magn. Reson. 83 (1989) 252.
[36] P.T. Callaghan, Principles of Nuclear Magnetic Resonance Microscopy, Clarendon Press, Oxford, 1991.
[37] H. Geen, S. Wimperis, R. Freeman, J. Magn. Reson. 85 (1989) 620.
[38] T.P.L.R. Roberts, PhD thesis, University of Cambridge, 1992.
[39] K. Raghavan, J.C. Park, S.J. Gibbs, Magn. Reson. Imag. 19 (2001) 697.
[40] G.L. Bretthorst, in: A. Mohammad-Djafari (Ed.), Maximum Entropy and Bayesian Methods, Kluwer, Dordrecht, 2001, in press.
[41] D.A. Nield, A. Bejan, Convection in Porous Media, 2nd ed, Springer, New York, 1999.
[42] S.J. Gibbs, K.L. James, L.D. Hall, D.E. Haycock, W.J. Frith, S. Ablett, J. Rheol. 40 (1996) 425.
[43] E.N. Lightfoot, J.L. Coffman, F. Lode, Q.S. Yaun, T.W. Perkins, T.W. Root, J. Chromatogr. A 760 (1997) 139.
[44] K.C.E. Ostergren, A.C. Tragardh, G.G. Enstad, J. Mosby, AIChE J. 44 (1998) 2.
[45] K. Schnitzlein, Chem. Eng. Sci. 56 (2001) 579.
[46] G.E. Mueller, Can. J. Chem. Eng. 75 (1997) 677.
[47] G.E. Mueller, Powder Technol. 72 (1992) 269.
[48] T. Elperin, E. Golshtein, Physica A 247 (1997) 67.